Nuclear Science and Techniques (2025) 36:78
https://doi.org/10.1007/s41365-025-01644-0

Gamma-induced positron beam generation at SLEGS

Sheng Jin[1,2] · Zi-Rui Hao[3] · Long-Xiang Liu[3] · Kai-Jie Chen[1,4] · Yu-Xuan Yang[1,5] · Hang-Hua Xu[3] · Yue Zhang[3] · Qian-Kun Sun[1,2] · Zhen-Wei Wang[1,2] · Gong-Tao Fan[1,2,3] · Hong-Wei Wang[1,2,3]

Received: 26 February 2024 / Revised: 26 June 2024 / Accepted: 5 July 2024 / Published online: 20 March 2025

Abstract
Energy-variable gamma-rays are produced in Laser Compton Slant-scattering mode at the Shanghai Laser Electron Gamma Source (SLEGS), a beamline of the Shanghai Synchrotron Radiation Facility (also called Shanghai Light Source). Based on the SLEGS energy-variable gamma-ray beam, a positron generation system composed of a gamma-ray-driven section, positron-generated target, magnet separation section and positron experimental section was designed for SLEGS. Geant4 simulation results show that the energy tunable positron beam in the energy range of 1–12.9 MeV with a flux of 3.7×10^4 –6.9×10^5 e^+/s can be produced in this positron generation system. The positron beam generation and separation provide favorable experimental conditions for conducting nondestructive positron testing on SLEGS in the future. The positron generation system is currently under construction and will be completed in 2025.

Keywords Shanghai Laser Electron Gamma Source · Monte Carlo simulation · Nondestructive testing · Positron · Geant4

1 Introduction

As the first antiparticle discovered by humans, positrons have been widely used in both basic and applied research. For example, positron beams with 10^{10} e^+/s high beam intensity and GeV energy are often employed as injection beams in large collider facilities [1]. Positron beams also play an important role in material performance testing combined with positron annihilation lifetime spectroscopy (PALS) [2–6] and coincidence Doppler broadening spectroscopy (CDBS) [7–9], among other technologies. Currently, there are four methods for obtaining positron beams: (1) ^{22}Na isotope source, isotope decay according to the reaction $^{22}\mathrm{Na} \rightarrow {}^{22}\mathrm{Ne} + \beta^+ + \nu_e$ [10, 11]; (2) positrons generated through an electromagnetic cascade shower process, where a heavy metal target is irradiated by high-energy electrons from an accelerator, such as LINAC [12–14]; (3) a heavy metal target irradiated by high-energy gamma-rays, called gamma-ray-driven positron source [15]; and (4) positrons generated by direct laser solid irradiation using an ultrahigh-power laser system, which has an ultrashort ps time structure [16, 17].

When determining the structural properties of materials using the positron nondestructive testing (NDT) method, the main requirements of the positron beam are as follows: (1) the positron energy must be adjustable to examine samples with different material densities and depths; (2) a high positron beam intensity is required for low detector efficiency; and (3) a positron beam spot must be selected to cover different sample sizes. Fortunately, a γ-ray-driven positron source based on a laser Compton scattering (LCS) gamma source meets all the above requirements, making it a good alternative for positron NDT [18].

This work was supported by the National Key Research and Development program (Nos. 2022YFA1602404, 2023YFA1606901), the National Natural Science Foundation of China (Nos. 12275338, 12388102, and U2441221), and the Key Laboratory of Nuclear Data foundation (JCKY2022201C152)xm.

✉ Gong-Tao Fan
fangt@sari.ac.cn

✉ Hong-Wei Wang
wanghw@sari.ac.cn

[1] Shanghai Institute of Applied Physics, Chinese Academy of Sciences, Shanghai 201800, China

[2] University of Chinese Academy of Sciences, Beijing 100080, China

[3] Shanghai Advanced Research Institute, Chinese Academy of Sciences, Shanghai 201210, China

[4] ShanghaiTech University, Shanghai 201210, China

[5] Zhengzhou University, Zhengzhou 450001, China

The LCS gamma source, which was first operated in the 1970 s, has the advantages of adjustable energy, quasi-monochromatic energy, adjustable flux and a beam spot. With the gamma-ray-driven method, the positron beam generated based on the LCS gamma source has the corresponding characteristics of adjustable energy, high beam intensity and a selectable beam spot. Because of these advantages, several renowned LCS gamma source facilities have been used for positron beam generation and application studies. The NewSUBARU BL01 LCS gamma source was used in a validation study of positron sources in 2019, and a positron beam with an intensity of 10^3 e^+/s was observed based on 16.9 MeV and 8.5×10^6 photons/s LCS gamma beams bombarding a lead target [19–21]. The UVSOR-III BL1U LCS gamma source also conducted a positron beam generation study using a γ-ray energy of approximately 6.6 MeV directly injected into a thick lead target, and a positron annihilation event rate of approximately 0.54 cps was measured [22]. Positron beam research is also planned for the ELI-NP LCS gamma branch (VEGA), which is still under construction in Romania [23–25].

The newly SLEGS LCS gamma source [26–30] at the Shanghai Synchrotron Radiation Facility (SSRF) has been available for users since 2023 and is the first LCS gamma source user device with a slant-scattering collision mode. According to the characteristics of the SLEGS' γ-ray beam [31, 32], a positron beam is planned for construction and conduct positron annihilation spectrum (PAS) research. A new positron beam with energy adjustability, high beam intensity and a selectable positron beam spot is currently under discussion.

In this paper, we provide a detailed description of the design, simulation and development of this new positron system. In Sect. 2, we briefly describe the SLEGS beamline and the parameters that must be considered. In Sect. 3, we describe the positron generation system design. Section 4 presents the simulation details. Section 5 describes the development status. Finally, Sect. 6 concludes the paper.

2 SLEGS beamline and its parameters

SLEGS is one of the new beamlines of the SSRF Project II (2016–2024) [33, 34]. SSRF is a third generation synchrotron radiation facility with a 3.5 GeV Stokes ring. The SSRF storage ring has two operating modes: top-up and single-bunch. When SSRF runs in top-up mode, four sets of electron trains in the storage ring, each with 125 consecutive bunches, are evenly spread in the 720 buckets [35]. When the SSRF runs in single-bunch mode, there is only one massive bunch in the storage ring [36].

Using a 10640 nm continuous CO_2 laser collision with 3.5 GeV electron in the SSRF storage ring, SLEGS produces MeV energy gamma-rays, which is the first LCS gamma source obtained by changing the collision angle between the laser and electron to obtain adjustable gamma energy [37–39]. The electron and laser beam parameter characteristics in SLEGS are listed in Table 1. The commissioning results show that the SLEGS gamma-ray energy range reaches 0.66–21.7 MeV (the Compton scattering maximum energy of the scattered gamma-ray spectrum). The gamma-ray bandwidth exceeds 2% with a tunable aperture of the collimator system (a ϕ1 mm collimator was used to obtain a 17 MeV gamma-ray with a laser electron collision angle of 124°) and will reach much more than 1% using a new type CO_2 laser in the near future. The flux reaches 4×10^7 photons/s under a 5 W CO_2 laser power and will reach nearly 10^8 photons/s with a 100 W CO_2 laser power in the future. The beam spot has an adjustable range of $\phi 1 - 25$ mm on the experimental target at a distance of approximately 40 m from the collision point. Particularly, the SLEGS gamma-ray beam has a time structure of less than 2 ps when the storage ring is operated in single-bunch mode.

3 Positron generation system design

Positron generation system is one of the most important application subsystems of the SLEGS beamline. The overall configuration of this system is shown in Fig. 1. It consists of γ-ray-driven section, positron-generated target, magnet separation section and PALS experimental section.

3.1 Gamma driven section

As a gamma-ray-driven positron beam, the properties of the gamma-ray will transmit to the radiated positron. For example, the energy and intensity of the driven gamma-ray will partly determine the radiated positron's energy and intensity. Furthermore, the bandwidth and time structure of the gamma-ray will directly determine the bandwidth and time structure of the generated positron [40]. To obtain a suitable

Table 1 Electron and laser beam parameters in SLEGS

Electron beam	Energy (GeV)	3.5
	Configuration	2 ps a bunch
	Top-up mode current (mA)	300
	Emittance ϵ_x/ϵ_y (nm rad)	4.2/0.042
	Beam radius σ_x/σ_y (μm)	138.3/6.12
CO_2 laser	Pulse width (μs)	50–1000
	Repetition rates (kHz)	1
	Wavelength (nm)	10640
	CW power (W)	5–100
	Beam radius ω (mm)	0.1–1

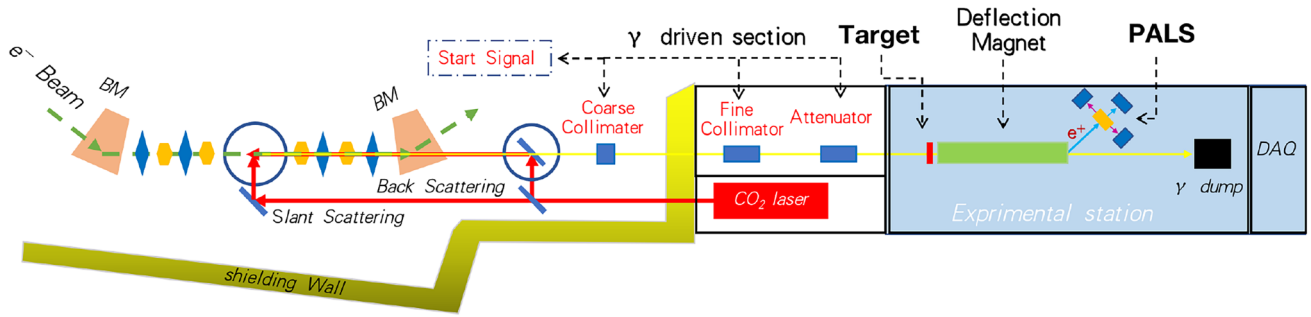

Fig. 1 (Color online) SLEGS beamline and positron beam configuration

gamma beam for positron generation, a gamma driven section is necessary. It is composed of a collimation and start signal subsection.

The collimation subsection consists of coarse and fine collimators which confines the emission angle of gamma-ray to less than 0.5 mrad along the beamline and adjusts the beam spot within 1–25 mm in diameter. Based on the SLEGS collimation subsection, continuous adjustment of both the gamma-ray bandwidth and gamma beam spot is achieved, meeting the requirement for generating high-quality positron beams. The details of the collimation subsection are given in reference [26].

The start signal is necessary for PALS with the order picosecond. The main part (BaF_2) of the PALS has been designed to routinely operate with beam durations of hundreds of picoseconds. Because of the fast response of the entire system, increasing the positron beam duration of a high-performance PALS will result in a decrease in resolution [41]. For higher resolution, it is preferable to have positron bunch duration that are significantly smaller than the timescales of interest, i.e., at least in the range of a few to tens of ps. In that case, the resolution of the system will be only limited by the detector response. This limitations can be overcome at SLEGS positron generation system if the SSRF run in single-bunch mode, with 10 ps pulse length and less than 2 ps jitters, combined with the continuously CO_2 laser, SLEGS can routinely generate high-intensity γ-ray pulse beams of 10-ps duration. Then positron bunch with a 10-ps duration can be obtained as the result of the electromagnetic cascade initiated by these gamma pulses as they propagate through a high-Z (mass number) converter target.

3.2 Positron generation target and separation section

The setup of the positron generation target and separation section is shown in Fig. 2. All targets can move in/out of the beam direction by a control mechanism. An electromagnet with tunable magnetic field is set just behind the target. The generated positron and electron are separated to opposite

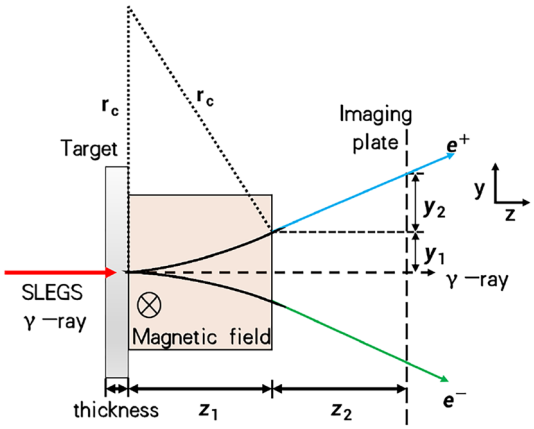

Fig. 2 Setup of the positron generation system (target, magnetic field, free flight distance and image plate, not in scale), see text for symbol description

directions, while the penetrated gamma-ray and scattering gamma-ray are not affected by the magnetic field and go forward along the beam direction.

The detailed process of the free positron beam generated as follows. First, the gamma-ray beam irradiates a positron generating target. Second, the gamma-ray is converted in the target to a positron and electron pair in the Coulomb field of the target nucleus. Third, the generated positron and electron inherit the momentum of gamma-ray, together with the unreacted gamma-ray enter a square uniform strong magnetic field with the dimension of z_1 for separating the positron and electron. The unreacted gamma rays pass through the magnetic field, while the positrons and electrons are separated from each other.

The separated free positron and electron will pass through a free flight distance of z_2 which is then recorded by an imaging plate with the position in the vertical direction of y_1, y_2 and deflection radius r_c, respectively. In order to obtain the positron beam with adjustable energy and flux, the magnetic field of the deflected electromagnet and the position z_2 of the imaging plate which determines the positron flight distance are designed to have a certain adjustment range. Detailed

parameters of the gamma driven section, generated target and separation section are listed in Table 2.

4 GEANT4 Monte Carlo simulation

The present simulation is based on the Geant4.10.04 version [42, 43] with the toolkit QGSP_BERT_HP which includes the G4EmStandardPhysics constructor describing electromagnetic process to determine the results of gamma transport and interaction. In the simulation, the LCS MeV energy γ-ray irradiates a high-Z target producing positron beam. Based on the Monte Carlo simulation, systemic analysis of the target, magnetic field and free flight distance have been carried out to achieve a high-yield, adjustable energy, narrow-bandwidth positron beam.

4.1 Typical gamma-ray and positron generation condition

The gamma-ray with a quasi-monoenergetic energy of 17 MeV (0.5% bandwidth), flux of 10^8 photons/s, $\phi 2$ (FWHM) spot size is performed in Fig. 3a and b. The reason for choosing this energy is that positron generation experiments at similar energies have been conducted in NewSUBARU BL01 [19, 44], also simulated with the EGS5 code, which can be used to verify the reliability of our simulation results.

Table 2 Parameters of positron generation and separation section

Target	Material	Be/Cu/Pb
	Purity (%)	100%
	Diameter (mm)	20
	Thickness (mm)	1.0−10.0
Electromagnet	Electromagnetic strength (Tesla)	0.1−0.5
	Electromagnetic gap, z_1 (mm)	100
	Field, length × width (mm^2)	100 × 100
Imaging plate	Size, length × width (mm^2)	400 × 400
	Position z_2 (mm)	0–600

A general positron production process has been carefully analyzed to obtain an effective analysis method. The modulated 17 MeV gamma-ray irradiates a 1 mm copper target, producing secondary particles, i.e., electron, positron and gamma-ray, and the energy spectra are shown in Fig. 4a. Figure 4b shows that the spatial distributions of the three particles are similar and overlapped when there is no electromagnetic separation section.

A yield of beryllium (Be), copper (Cu) and lead (Pb) targets was calculated with the different thicknesses shown in Fig. 5. On the one hand, the high-Z target is required to improve the yield of the electron pair effect, and on the other hand, the gamma background is caused by the scattering of high-Z materials; thus, the optimized signal-to-noise ratio of positron should be considered with material.

We apply a constant magnetic field of 0.1–0.5 Tesla in the magnetic field area. Figure 6 shows that the magnetic field in the y direction separates the positron and electron. After passing through the magnetic field and transmitting a distance of 400 mm, the positron beam spot expands further to $\phi 50$ (in FWHM). The distribution of positron and electron is symmetrically separated along the y direction. The unreacted gamma is still distributed along the propagation direction, but secondary gamma will lead to more background.

In order to effectively reflect the quality of the generated positron beam, the signal-to-noise ratio (SNR) parameter is employed. SNR is defined as the ratio of positron yield to background gamma yield at a certain measurement position, which is a complicated result of several factors, such as the position in y direction, incident gamma energy (E), target thickness (t), magnetic field (B), magnetic field range

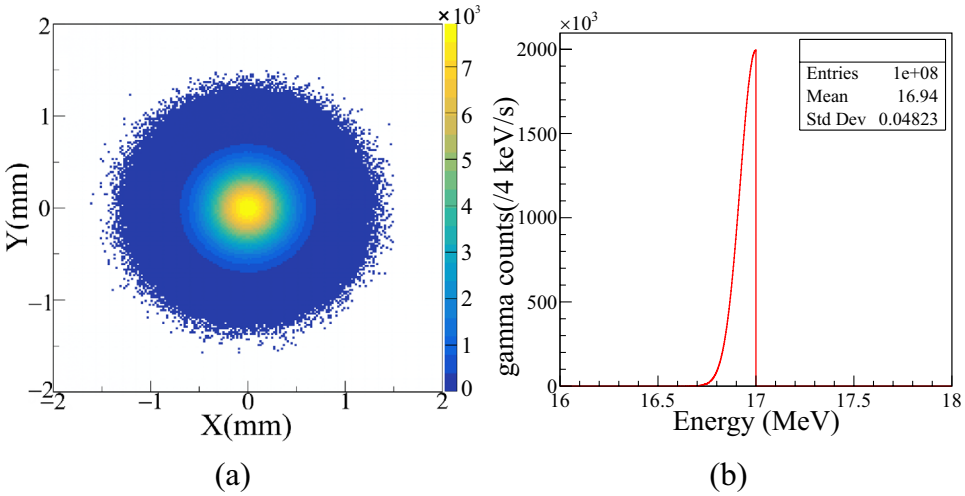

Fig. 3 Quasi-monoenergetic 17 MeV gamma-ray beam spots (**a**) and beam spectrum before the target (**b**)

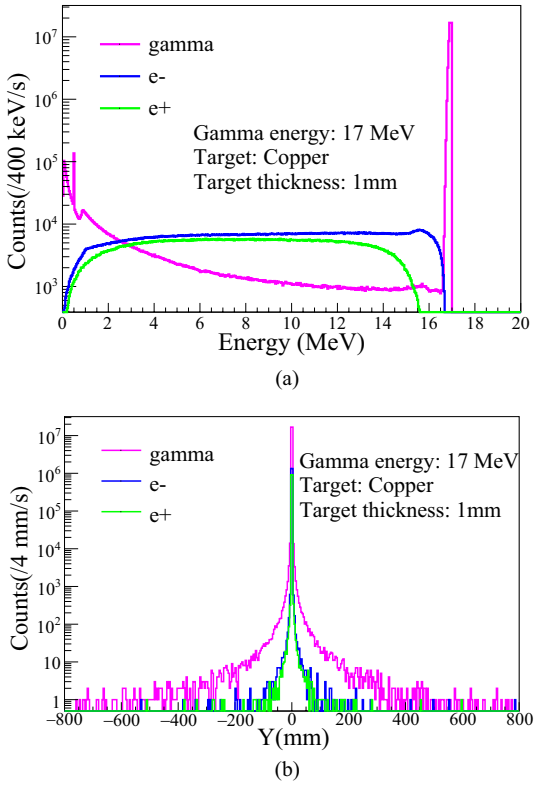

Fig. 4 Energy distributions of positron, electron and gamma-ray (**a**), spatial distribution without magnet separation (**b**)

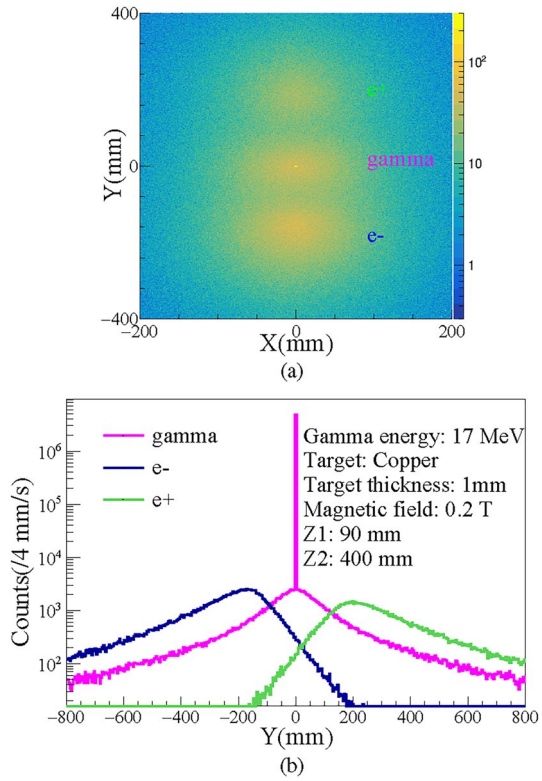

Fig. 6 (Color online) Beam spatial distribution after magnet separated (**a**) and projection of the beam spatial distribution onto the *y*-axis at 0.2 T (**b**)

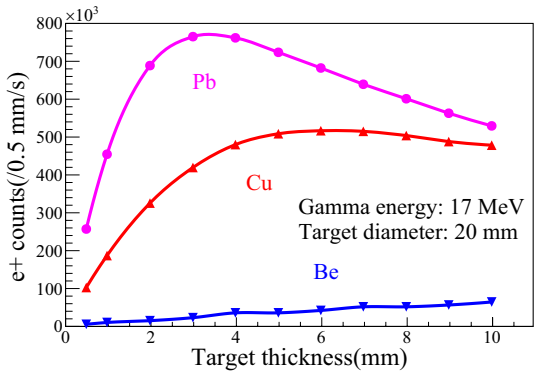

Fig. 5 Normal positron yield with Be, Cu and Pb target

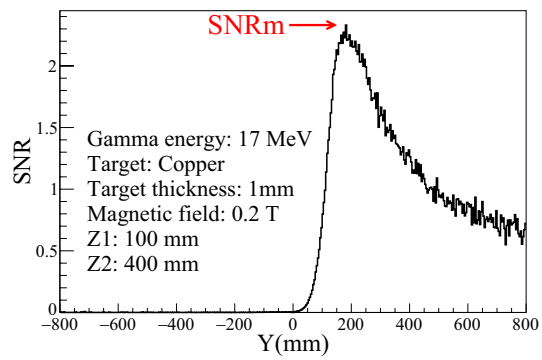

Fig. 7 SNR distribution in the y direction as well as the SNRm

(z_1) and free flight distance (FFD) (z_2). Then the SNR peak (written as SNRm) value, which is defined as the maximum of SNR, can reflect the optimized value of positron yield with a set of parameters (E, t, B, z_1, z_2). The SNR distribution, a function of y direction, using the previous parameters (E: 17 MeV, t:1 mm, B: 0.2 T, z_1: 100 mm, z_2: 400 mm) is shown in Fig. 7.

Figure 8 shows that judged by the SNRm, the optimized target thickness obtained by taking into account the contribution of gamma background is the 0.5–1.5-mm-thick copper target, while the lead target with the same thickness does not have the optimal signal-to-noise ratio because of the strong gamma scattering effect.

4.2 Determination of positron generation system parameters

Considering a practical positron generation process even further, in order to obtain a high-quality positron beam with high flux, low background, narrow bandwidth, etc., a

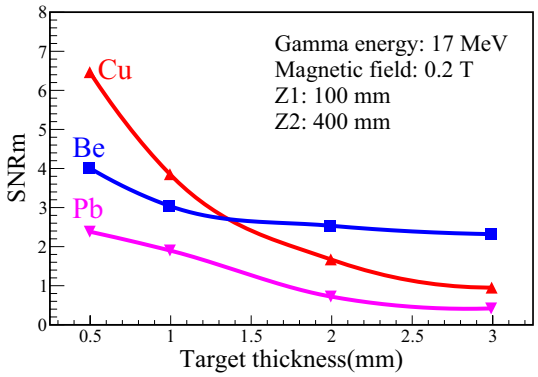

Fig. 8 SNRm distribution as a function of the target thickness

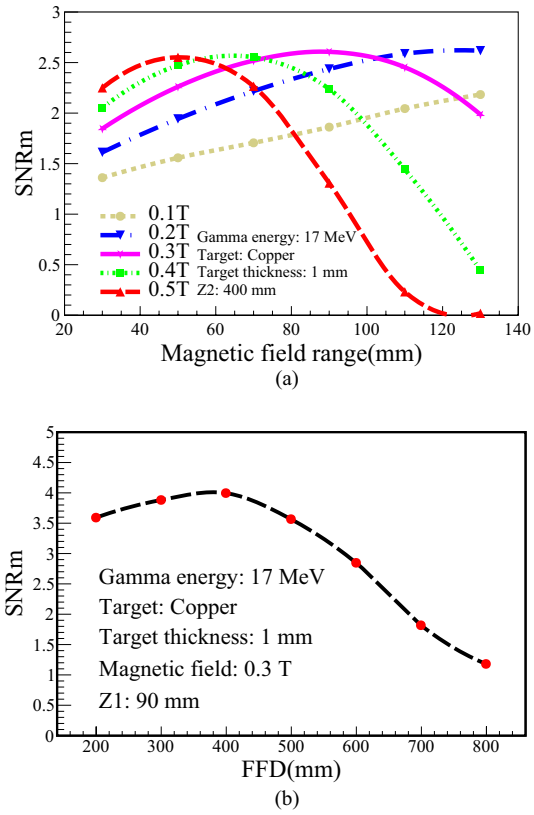

Fig. 9 (Color online) Relationship between SNRm, magnetic induction intensity and FFD. **a** SNRm and magnetic induction intensity; **b** SNRm and FFD

systematic consideration of target thickness, magnetic field size, magnetic field strength and flight distance is required to be optimized for the positron beam.

4.2.1 Target

There are two main target parameters affecting the positron properties: the target material and its thickness. The positron yield gradually dominates as the Z value increases, but too large Z value will also lead to the secondary gamma background increase, which is detrimental the signal-to-noise of positron. If the target thickness is too small, the occurrence of the positron yield will decrease, while if thickness is too large, the scattered gamma background will increase significantly and the scattering of the positron in target will also lead to worse SNR. The positron spillover yield of whatever target materials decreases with the increasing target thickness.

Then generated positron passed through a 0.1–0.5 T magnetic field with variable length, and the variation of SNRm of the three generated targets as a function of the target thickness is shown in Fig. 8. It can be seen that the SNRm decreases as the thickness of the target increases. In the thin target region, less than 1.3 mm, the Cu target has the largest SNRm while Pb has the smallest SNRm. In the thick target region, larger than 1.3 mm, the Be has the highest SNRm and the Pb still has the lowest SNRm. The SNRm of the Be and Cu crosses at 1.3 mm. Combined with the yield and SNRm, the 1-mm-thick Cu is finally chosen as the positron generating target at the parameters (E: 17 MeV, B: 0.2 T, z_1: 100 mm, z_2: 400 mm).

4.2.2 Magnetic field

The magnetic field also has two characteristic parameters, the field range (z_1) and the magnetic induction intensity (B), which need to be considered together. Figure 9a shows a small area with high magnetic induction intensity has a similar effect to a large area with low magnetic induction intensity. At the same time, too high magnetic induction intensity will cause positron to move in a circular motion within the magnetic field and cannot reach the receiver plate. Too low magnetic induction intensity will cause the deflection distance (y_1) too small and the positron will still be mixed with the scattered gamma background, which will not be improved SNR.

As shown in Fig. 9a, a wider magnetic field range (i.e., the z_1 value in Fig. 2) is required for weak magnetic strengths of 0.1 T and 0.2 T. On the contrary, a small magnetic field area is enough for strong magnetic strengths of 0.4 T and 0.5 T. A maximum SNRm value appears at 90–100 mm magnetic field range (z_1) under 0.3 T. Finally, the parameters of the magnetic field are taken as 0.3 T and 90 mm (E: 17 MeV, t: 1 mm, B:0.3 T, z_1: 90 mm).

4.2.3 Free flight distance (FFD)

The free flight distance is the projection length of the transmitting path of the positron on the z-axis after passing through the magnetic field. After gaining deflection momentum in the magnetic field, the positron transmits out

of the magnetic field region and continues to transmit in the y-axis direction in the free flight region. Since the positron energy distribution has a certain width, the deflection in the magnetic field will lead to further divergence of the positron beam spot, and the free flight distance should not be too large to obtain a suitable positron SNR and beam spot size. We also use SNRm to characterize the quality of positron beam after passing through different free flight regions, and Fig. 9b shows that the SNRm reaches its maximum at a free flight distance of 400 mm (E: 17 MeV, t: 1 mm, B: 0.3 T, z_1: 90 mm, z_2: 400 mm).

4.2.4 Beam qualities

Combined with the settings mentioned in the previous section (E: 17 MeV, t: 1 mm, B: 0.3 T, z_1: 90 mm, z_2: 0 mm), the positron beam qualities at the target point have been analyzed carefully. The simulated positron beam is symmetrical in x direction and similar to Lorentz distribution in y direction, as shown in Fig. 10a and b. The beam spot size increases following the y direction. Mean energy of the positron spectrum is near 11 MeV with a 74% wide bandwidth. And the positron beam intensity is better than 8.9×10^5 e^+/s.

The positron beam is further investigated with a collimator. The simulated energy distributions of positron beam that are filtered by an edge length 15 mm, lead, square collimator will be improved. A positron beam of 11.9 MeV with 45% bandwidth is achievable for the square collimator with placement at $y \in (23.7, 38.7)$, $x \in (-7.5, 7.5)$ the intensity of 1.2×10^5 e^+/s.

4.3 Positron beam properties in SLEGS

In the previous section, as a typical example, the process of producing a positron beam based on a 17 MeV gamma beam is carefully simulated in SLEGS. The positron beam with mean energy of 11.9 MeV has the bandwidth better than 45% and the intensity is more than 10^5 e^+/s. The energy of the quasi-monochromatic gamma beam at SLEGS can continuously adjusted from 0.66 MeV to 21.7 MeV with a slant Compton scattering method. Following the previous method, the simulation of producing positron beams based on different energy gamma beams has been carried out carefully. The positron beam spectrum at different energy gamma beams is shown in Fig. 11.

From Fig. 11, as the incident γ-ray beam energy increases, the mean energy and flux (corresponding the spectrum integral area) of positron beam increases. The incident γ -ray beam energy varies in a wide range from 3.0 MeV to 21.0 MeV. In this range, the mean energy of positron beam varies from 1 MeV to 12.9 MeV, with the flux from 3.7×10^5 e^+/s to 6.9×10^5 e^+/s and the energy resolution of

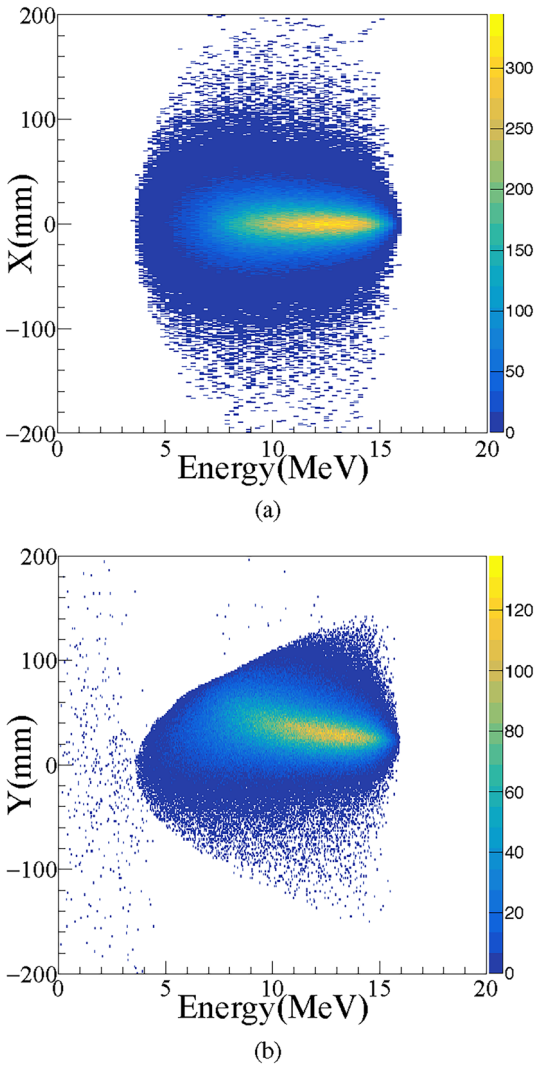

Fig. 10 (Color online) Position energy distribution in the X–Y direction at the parameters of (E: 17 MeV, t: 1 mm, B: 0.3 T, z_1: 90 mm, z_2: 0 mm)

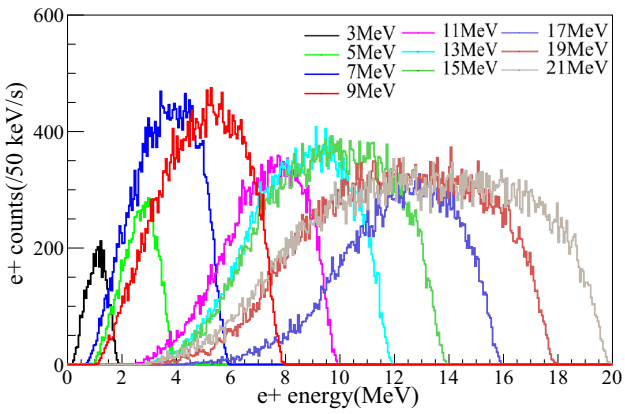

Fig. 11 (Color online) Positron energy spectrum at varying incident gamma energy

near 40% in FWHM by using a square collimator with side length of 15 mm aperture.

5 Development status

As a construction project, the positron beam generation system in SLEGS has been funded. The gamma driven section including collimation and start signal subsection is part of the SLEGS beam line and has been built. As an independent subsystem, the PALS system has also been built separately.

The separated positron beam travels nearly 400 mm before reaching the sample. A new SLEGS PALS was designed to achieve high-level measurement using positron beam as shown in Fig. 12a. The PALS consists of two BaF_2 (ϕ51 mm × 20 mm, highly polished) scintillator detectors, one set of data acquisition devices, including the digital waveform processing module APV8002 from TechnoAP in Japan, the time measurement module APV8702, the high-voltage module APV3003 and the front-end amplifier power supply module APV4004. The 10-ps duration gamma-ray pulse provides the start signal for the positron lifetime measurement. The stop signal consists of annihilation gamma-rays that are emitted back-to-back from the sample at 0.511 MeV. Detector-2 records the gamma-ray pulse signal, while detector-1 measures the annihilation gamma-ray of 0.511 MeV. Then, the time difference between incident gamma and annihilated gamma is recorded. In our design scheme, the start signal will come from the triggering time of laser pulses, high-frequency signals of electron beams or direct measurements of gamma beams.

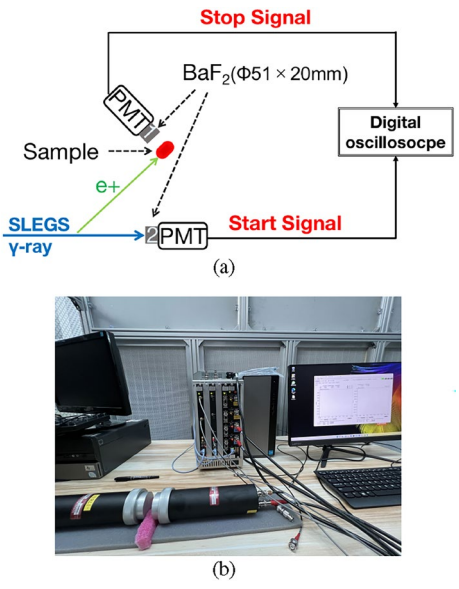

Fig. 12 (Color online) Schematics of PALS for positron life time measurements (**a**) and PALS setup (**b**)

Specialized data acquisition software for PALS is available in lifetime, energy, coincidence Doppler broadening (CDB) and age–momentum correlation (AMOC) operating modes, allowing for the measurement of time and energy, where HPGe, BaF_2 and $LaBr_3$ are used for the measurements. By feeding the response signal of the HPGe detector at ^{60}Co to the digital waveform processing module APV8002, the acquisition parameters are configured to measure the energy resolution. The energy resolution of ~0.2% at 1.332 MeV is obtained from the data acquisition. The picture of PALS setup is shown in Fig. 12b. By placing ^{60}Co between the two scintillator detectors $LaBr_3$, the detector signal is sent to the time measurement module APV8702, which is configured to obtain parameters to measure the time resolution. The time resolution is 159.3 ps.

The basic test experiment has been completed by choosing to inject 13 MeV gamma-rays into a 1 cm lead target at a flux of 7×10^4 photons/s for a measurement time of one hour. The positrons will annihilate in the target and a measurement of 511 keV of gamma-rays will emit a positron yield. Seven $LaBr_3$ detectors were used in the experiment to measure the resulting 511 keV. Considering the detection efficiency of $LaBr_3$ detector and the effect of the stereo angle, the total number of 511 keV in the full space was calculated to be 2.5×10^8 photons/h. Gamma-rays and a 1 cm lead target are added to the simulation. Secondary gamma-rays of 511 keV are collected in full space, and the total number obtained is 2.47×10^8 photons/h, which is basically consistent with the experimental results. Verify the reliability of the simulation under these conditions.

6 Conclusion

This paper introduces the positron generation system designed for the SLEGS beamline in detail. The positron generation system consists of γ-ray-driven section, positron-generated target, magnet separation section and PALS experimental section. It will generate a new type of positron beam based on the gamma beams of SLEGS. Monte Carlo simulations have been carried out to analyze positron energy, beam flux and spot sizes resulting from positron-generated target and magnet separation section of the positron generation system. The result shows that the incident gamma energy, flux, bandwidth, targets, magnetic field and free flight distance are directly related to the positron energy, beam flux and spot sizes. The recommended quasi-monochromatic positron beams are produced in the energy range of 1–12.9 MeV with a flux of 3.7×10^4 e^+/s to 6.9×10^5 e^+/s and an energy resolution of near 40% in FWHM.

Now the positron generation system is under construction in SLEGS. The gamma driven section and start signal subsection are part of the SLEGS beam line and have been

built. The PALS system has also been built separately and carried out the test run. Based on the simulation work of this paper, both positron-generated target and magnet separation section have been designed and are in the process of equipment manufacturing. Experimental measurements have been taken, and annihilation gamma-ray count rates have been measured using detector arrays, which are consistent with simulations of the calculated positron intensity and expected annihilation gamma-ray counts. The entire positron generation system is expected to be completed by 2025.

Author contributions All authors contributed to the research idea and design of this article. Sheng Jin was responsible for writing the procedures, conducting the experiments, compiling the results, analyzing the data and drafting and revising the final version of the article. Hong-Wei Wang and Gong-Tao Fan were responsible for the overall guidance of the protocol, critical review and revision of the article. Yue Zhang, Zi-Rui Hao, Hang-Hua Xu, Long-Xiang Liu, Yu-Xuan Yang, Kai-Jie Chen, Qian-Kun Sun and Zhen-Wei Wang were involved in the experimental process as well as the discussion and revision of the article.

Data availability The data that support the findings of this study are openly available in Science Data Bank at https://cstr.cn/?31253.11.sciencedb.j00186.00504 and https://www.doi.org/10.57760/sciencedb.j00186.00504.

Declarations

Conflict of interest The authors declare that they have no conflict of interest.

References

1. H. Nagoshi, M. Kuribayashi, M. Kuriki et al., A design of an electron driven positron source for the internationallinear collider. Nucl. Instrum. Meth. A. **953**, 163134 (2020). https://doi.org/10.1016/j.nima.2019.163134
2. Q. Zhao, R. Ye, H. Wang et al., A multi-parameter discrimination digital positron annihilation lifetime spectrometer using a fast digital oscilloscope. Nucl. Instrum. Methods A **1023**, 165974 (2021). https://doi.org/10.1016/j.nima.2021.165974
3. R.E. Bell, R.L. Graham, Time distribution of positron annihilation in liquids and solids. Phys. Rev. **90**, 644–654 (1953). https://doi.org/10.1103/PhysRev.90.644
4. M.M. Hu, J.J. Liu, J.J. Kong et al., Free volume and gas transport properties of hydrolyzed polymer of intrinsic microporosity (PIM-1) membrane studied by positron annihilation spectroscopy. Micropor. Mesopor. Mat. **335**, 111770 (2022). https://doi.org/10.1016/j.micromeso.2022.111770
5. T. Zhu, B.Y. Wang, X.Y. Lian et al., Positron annihilation spectroscopy characterization of formation of Helium/Hydrogen-vacancy nano-clusters in FeCr alloy. Acta Phys. Pol. A **137**, 235–237 (2020). https://doi.org/10.12693/aphyspola.137.235
6. Q.H. Zhao, X.X. Han, H.B. Wang et al., A new digital positron annihilation lifetime spectrometer for a single piece of micron-thickness film. Nucl. Instrum. Methods A **1038**, 166921 (2022). https://doi.org/10.1016/j.nima.2022.166921
7. J. Cizek, M. Viček, I. Prochazka, Digital spectrometer for coincidence measurement of doppler broadening of positron annihilation. Nucl. Instrum. Methods A **623**, 982–994 (2010). https://doi.org/10.1016/j.nima.2010.07.046
8. Z.Q. Chen, X.J. Hu, S.Y. Wang, Vacancies and impurities in inp studied using positron lifetime and an improved doppler-broadening spectrometer. Appl. Phys. A **66**, 435–440 (1998). https://doi.org/10.1007/S003390050690
9. M. Müller, A. Rempel, K. Reichle et al., Identification of vacancies on each sublattice of SiC by coincident doppler broadening of the positron annihilation photons after electron irradiation. Mater. Sci. Forum **363–365**, 70–72 (2001). https://doi.org/10.4028/www.scientific.net/MSF.363-365.70
10. M.S. Basunia, Nuclear data sheets for $A = 22$. Nucl. Data Sheets **127**, 69–190 (2015). https://doi.org/10.1016/j.nds.2015.07.002
11. L.H. Cong, B.C. Gu, X.X. Han et al., Symmetrical positron annihilation lifetime spectrometer and single-sided measurements. J. Instrum. **14**, P10021 (2019). https://doi.org/10.1088/1748-0221/14/10/P10021
12. M. Inoue, S. Takenaka, K. Yoshida et al., Experiment of positron generation using a crystal target at the KEK electron/positron linac. Nucl. Instrum. Methods Phys. Res. Sect. B **173**, 104–111 (2001). https://doi.org/10.1016/S0168-583X(00)00195-6
13. Z.T. Zhao, D. Wang, Z.Y. Yang et al., Sclf: an 8-GeV CW SCRF linac-based X-ray FEL facility in Shanghai. https://doi.org/10.18429/JACOW-FEL2017-MOP055
14. Y. Enomoto, H. Saotome, M. Satoh et al., A new pulse magnet control system in the KEK electron positron LINAC. (2018). https://doi.org/10.18429/JACOW-IPAC2018-WEPAK014
15. C. Hugenschmidt, K. Schreckenbach, D. Habs et al., High-intensity and high-brightness source of moderated positrons using a brilliant γbeam. Appl. Phys. B **106**, 241–249 (2012). https://doi.org/10.1007/s00340-011-4594-0
16. T.L. Audet, A. Alejo, L. Calvin et al., Ultrashort mev-scale laser-plasma positron source for positron annihilation lifetime spectroscopy. Phys. Rev. Accel. Beams (2021). https://doi.org/10.18429/JACOW-IPAC2018-WEPAK014
17. J. Zhao, Y.T. Hu, Y. Lu et al., All-optical quasi-monoenergetic GeV positron bunch generation by twisted laser fields. Commun. Phys. **5**, 1–10 (2022). https://doi.org/10.1038/s42005-021-00797-9
18. Z.Q. Chen, J.J. Shi, J.C. Jiang et al., A modified positron lifetime spectrometer as method of non-destructive testing in materials. Appl. Surf. Sci. **327**, 418–423 (2015). https://doi.org/10.1016/j.apsusc.2014.11.114
19. K. Sugita, S. Miyamoto, M. Terasawa et al., Development of a positron annihilation measurement system by implantation of 17 MeV gamma beam into bulk materials. AIP Conf. Proc. **2182**, 040007 (2019). https://doi.org/10.1063/1.5135839
20. F. Hori, K. Ishii, T. Ishiyama et al., Production of positrons via pair creation from LCS gamma-rays and application to defect study in bulk materials. In *JJAP Conference Proceedings* . https://doi.org/10.7567/JJAPCP.2.011301
21. D. Li, K. Imasaki, S. Miyamoto et al., Positron generation through laser compton scattering gamma ray. Appl. Phys. Lett. **94**, 1112–091112 (2009). https://doi.org/10.1063/1.3094882
22. Y. Taira, H. Toyokawa, R. Kuroda et al., Photon-induced positron annihilation lifetime spectroscopy using ultrashort laser-compton-scattered gamma-ray pulses. Rev. Scientific Instrum. **84**, 053305 (2013). https://doi.org/10.1063/1.4807701
23. N. Djourelov, A. Oprisa, V. Leca, Source of slow polarized positrons using the brilliant gamma beam at ELI-NP. converter design and simulations. Nucl. Instrum. Methods A **806**, 146–153 (2016). https://doi.org/10.1016/j.nima.2015.10.009
24. N. Djourelov, A. Oprisa, D. Dinescu et al., Status of the project for a positron laboratory at ELI-NP. J. Phys. Conf. Ser. **791**, 012011 (2017). https://doi.org/10.1088/1742-6596/791/1/012011
25. N. Djourelov, D. Dinescu, Design and simulation of a pulsed positron beam at ELI-NP. J. Phys. Conf. Ser. **791**, 012010 (2017). https://doi.org/10.1088/1742-6596/791/1/012010

26. Z.R. Hao, G.T. Fan, H.W. Wang et al., Collimator system of SLEGS beamline at shanghai light source. Nucl. Instrum. Methods A **1013**, 165638 (2021). https://doi.org/10.1016/j.nima.2021.165638
27. H.H. Xu, J.H. Chen, G.T. Fan et al., Interaction chamber design for a Sub-MeV laser-compton gamma-ray source. https://doi.org/10.18429/JACOW-IPAC2015-TUPJE021
28. Z.R. Hao, G. Fan, H. Xu et al., Quasi-monochromatic gamma beam modulation at SLEGS. Radiat. Meas. **174**, 107127 (2024). https://doi.org/10.1016/j.radmeas.2024.107127
29. H.H. Xu, G.T. Fan, H.W. Wang et al., Interaction chamber for laser compton slant-scattering in SLEGS beamline at shanghai light source. Nucl. Instrum. Methods A **1033**, 166742 (2022). https://doi.org/10.1016/j.nima.2022.166742
30. H.W. Wang, G.T. Fan, L.X. Liu et al., Development and prospect of Shanghai laser Compton scattering Gamma source. https://doi.org/10.11804/NUCLPHYSREV.37.2019043
31. H.W. Wang, G.T. Fan, L.X. Liu et al., Commissioning of laser electron gamma beamline SLEGS at SSRF. Nucl. Sci. Tech. **33**, 87 (2022). https://doi.org/10.1007/s41365-022-01076-0
32. Y.X. Yang, W. Zhao, X.G. Cao et al., Simulation study on the production of medical radioisotopes ^{186g}Re by photonuclear reaction. Radiat. Phys. Chem. **218**, 111599 (2024). https://doi.org/10.1016/j.radphyschem.2024.111599
33. H.J. Xu, Z.T. Zhao, Current status and progresses of SSRF project. Nucl. Sci. Tech. **19**, 1–6 (2008). https://doi.org/10.1016/S1001-8042(08)60013-5
34. X. Wu, S.Q. Tian, X.Z. Liu et al., Design and commissioning of the new SSRF storage ring lattice with asymmetric optics. Nucl. Instrum. Methods A **1025**, 166098 (2022). https://doi.org/10.1016/j.nima.2021.166098
35. X.Y. Xu, Y.B. Leng, Y.M. Zhou et al., Bunch-by-bunch three-dimensional position and charge measurement in a storage ring. Phys. Rev. Accel. Beams **24**, 032802 (2021). https://doi.org/10.1103/PhysRevAccelBeams.24.032802
36. J. He, M. Liu, C.X. Yin et al., Experimental studies on the x-ray single-pulse jitter at the SSRF. Nucl. Instrum. Methods A **1025**, 166038 (2022). https://doi.org/10.1016/j.nima.2021.166038
37. K.J. Chen, L.X. Liu, Z.R. Hao et al., Simulation and test of the SLEGS TOF spectrometer at SSRF. Nucl. Sci. Tech. **34**, 47 (2023). https://doi.org/10.1007/s41365-023-01194-3
38. L.X. Liu, H. Utsunomiya, G. Fan et al., Energy profile of laser Compton slant-scattering γ-ray beams determined by direct unfolding of total-energy responses of a BGO detector. Nucl. Instrum. Methods A **1063**, 169314 (2024). https://doi.org/10.1016/j.nima.2024.169314
39. D.X. Wang, S. Zhang, X.R. Hu et al., Light output of EJ299-33A scintillator and its application. Nucl. Tech. (in Chinese) **45**, 020403 (2022). https://doi.org/10.11889/j.0253-3219.2022.hjs.45.020403
40. D. Schödlbauer, P. Sperr, G. Kögel et al., A pulsing system for low energy positrons. Nucl. Instrum. Methods Phys. Res. Sect. B **34**, 258–268 (1988). https://doi.org/10.1016/0168-583X(88)90752-5
41. S. Van Petegem, B. Waeyenberge, D. Segers et al., A high-performance, high-resolution positron annihilation coincidence doppler broadening spectrometer. Nucl. Instrum. Methods A **513**, 622–630 (2003). https://doi.org/10.1016/j.nima.2003.06.001
42. J. Allison, K. Amako, J. Apostolakis et al., Geant4 developments and applications. IEEE Trans. Nucl. Sci. **53**, 270–278 (2006). https://doi.org/10.1109/TNS.2006.869826
43. S. Agostinelli, J. Allison, K. Amako et al., Geant4–a simulation toolkit. Nucl. Instrum. Meth. A. **506**, 250–303 (2003). https://doi.org/10.1016/S0168-9002(03)01368-8
44. K. Ito, N. Kadoya, Y. Katsuta et al., Evaluation of the electron transport algorithm in magnetic field in EGS5 Monte Carlo code. Phys. Med.: PM: Int. J. Devot. Appl. Phys. Med. Biol.: Off. J. Ital. Assoc. Biomed. Phys. **93**, 46–51 (2021). https://doi.org/10.1016/j.ejmp.2021.12.001